UNIVERSITY OF AMSTERDAM

UvA-DARE (Digital Academic Repository)

Evidence for a TDE origin of the radio transient Cygnus A-2

de Vries, M.N.; Wise, M.W.; Nulsen, P.E.J.; Siemiginowska, A.; Rowlinson, A.; Reynolds, C.S.

DOI
10.1093/mnras/stz1078

Publication date
2019

Document Version
Final published version

Published in
Monthly Notices of the Royal Astronomical Society

License
CC BY-NC

Link to publication

Citation for published version (APA):
de Vries, M. N., Wise, M. W., Nulsen, P. E. J., Siemiginowska, A., Rowlinson, A., & Reynolds, C. S. (2019). Evidence for a TDE origin of the radio transient Cygnus A-2. *Monthly Notices of the Royal Astronomical Society*, *486*(3), 3388-3401. https://doi.org/10.1093/mnras/stz1078

General rights
It is not permitted to download or to forward/distribute the text or part of it without the consent of the author(s) and/or copyright holder(s), other than for strictly personal, individual use, unless the work is under an open content license (like Creative Commons).

Disclaimer/Complaints regulations
If you believe that digital publication of certain material infringes any of your rights or (privacy) interests, please let the Library know, stating your reasons. In case of a legitimate complaint, the Library will make the material inaccessible and/or remove it from the website. Please Ask the Library: https://uba.uva.nl/en/contact, or a letter to: Library of the University of Amsterdam, Secretariat, P.O. Box 19185, 1000 GD Amsterdam, The Netherlands. You will be contacted as soon as possible.

UvA-DARE is a service provided by the library of the University of Amsterdam (https://dare.uva.nl)

Download date:11 Oct 2026

Monthly Notices
of the
ROYAL ASTRONOMICAL SOCIETY

MNRAS **486,** 3388–3401 (2019)
Advance Access publication 2019 April 16

doi:10.1093/mnras/stz1078

Evidence for a TDE origin of the radio transient Cygnus A-2

M. N. de Vries,[1]★ M. W. Wise,[1,2]★ P. E. J. Nulsen,[3,4]★ A. Siemiginowska,[3] A. Rowlinson[1,5] and C. S. Reynolds[6]

[1]*Astronomical Institute 'Anton Pannekoek', University of Amsterdam, Science Park 904, NL-1098 XH Amsterdam, the Netherlands*
[2]*SRON Netherlands Institute for Space Research, Sorbonnelaan 2, NL-3584 CA Utrecht, the Netherlands*
[3]*Harvard-Smithsonian Center for Astrophysics, 60 Garden Street, Cambridge, MA 02138, USA*
[4]*ICRAR, University of Western Australia, 35 Stirling Hwy, Crawley WA 6009, Australia*
[5]*ASTRON, Netherlands Institute for Radio Astronomy, Postbus 2, NL-7990 AA Dwingeloo, the Netherlands*
[6]*Institute of Astronomy, University of Cambridge, Cambridge CB3 0HA, UK*

Accepted 2019 April 11. Received 2019 March 26; in original form 2019 January 31

ABSTRACT

In 2015, a radio transient named Cygnus A-2 was discovered in Cygnus A with the Very Large Array. Because of its radio brightness ($\nu F_\nu \approx 6 \times 10^{39}$ erg s^{-1}), this transient likely represents a secondary black hole in orbit around the active galactic nucleus. Using *Chandra* ACIS observations from 2015 to 2017, we have looked for an X-ray counterpart to Cygnus A-2. The separation of 0.42 arcsec means that Cygnus A-2 cannot be spatially resolved, but by comparing the data with simulated MARX data, we put an upper limit to the 2–10 keV X-ray luminosity of Cygnus A-2 of 1×10^{43} erg s^{-1}. Using the Fundamental Plane for accreting black holes, we find that our upper limit to the X-ray flux of Cygnus A-2 in 2015–2017 disfavours the interpretation of Cygnus A-2 as a steadily accreting black hole. We suggest instead that Cygnus A-2 is the radio afterglow of a tidal disruption event (TDE) and that a peak in the 2–10 keV luminosity of the nuclear region in 2013, when it was observed by *Swift* and *NuSTAR*, is X-ray emission from the TDE. A TDE could naturally explain the X-ray light curve of the nuclear region, as well as the appearance of a short-lived, fast, and ionized outflow previously detected in the 2013 *NuSTAR* spectrum. Both the radio and X-ray luminosities fall in between typical luminosities for 'thermal' and 'jetted' TDE types, suggesting that Cygnus A-2 would be unlike previously seen TDEs.

Key words: galaxies: active – galaxies: individual: Cygnus A – X-rays: galaxies.

1 INTRODUCTION

The central engine of the radio-bright galaxy Cygnus A is generally understood to be a heavily obscured, broad-line active galactic nucleus (AGN; Antonucci, Hurt & Kinney 1994; Ueno et al. 1994; Ogle et al. 1997). Because of the heavy obscuration by the giant elliptical host galaxy, the AGN is not directly visible at optical, UV and soft X-ray wavelengths (Young et al. 2002; Canalizo et al. 2003). In contrast to the extreme radio power of the galaxy, the AGN itself is only moderately luminous with a bolometric luminosity $L_{\rm Bol} = 10^{45}$ erg s^{-1} (Privon et al. 2012).

In 2015 July, Perley et al. (2017) discovered a transient point source in Cygnus A with the Karl G. Jansky Very Large Array (VLA). The transient, named Cygnus A-2, is located 0.42 arcsec (460 pc) southwest of the primary AGN. Follow-up observations in 2016 with VLA and the Very Long Baseline Array (VLBA) confirmed the presence of the source, and the flux and spectral shape showed no obvious variability within that year. The transient was not observed in previous VLA observations, most recently in 1997, and therefore appeared sometime between 1997 and 2015.

The radio luminosity $\nu F_\nu \approx 6 \times 10^{39}$ erg s^{-1} makes Cygnus A-2 a rather bright radio transient. The high luminosity puts a strong constraint on the origin of Cygnus A-2. Perley et al. (2017) investigated whether Cygnus A-2 could be the radio afterglow of a supernova, although a supernova with such a high radio luminosity would be a rare and unlikely event. The favoured explanation is that Cygnus A-2 is a secondary black hole, orbiting the primary AGN. The black hole could have brightened due to a steady increase in accreting material in the past 20 yr, or through the sudden disruption of a star by the black hole, known as a tidal disruption event (TDE).

A point source coinciding with the location of Cygnus A-2 was observed in the infrared with the *Keck* II AO system in 2003

★ E-mail: martijndevries91@gmail.com (MNdeV); m.wise@uva.nl (MWW); pnulsen@cfa.harvard.edu (PEJN)

© 2019 The Author(s)
Published by Oxford University Press on behalf of The Royal Astronomical Society. This is an Open Access article distributed under the terms of the Creative Commons Attribution Non-Commercial License (http://creativecommons.org/licenses/by-nc/4.0/), which permits non-commercial re-use, distribution, and reproduction in any medium, provided the original work is properly cited.

Downloaded from https://academic.oup.com/mnras/article-abstract/486/3/3388/5470967 by Universiteit van Amsterdam user on 13 March 2020

Table 1. Overview of previously measured X-ray properties of the AGN, measured by three different X-ray instruments.

Date	Ref.	Instrument	N_H (10^{23} cm^{-2})	$L_{2-10\mathrm{keV}}$ (erg s^{-1})	Γ
2000 05	1	*Chandra* ACIS	$2.0^{+0.2}_{-0.1}$	1.9×10^{44}	$1.52^{+0.12}_{-0.12}$
2005 10	2	*XMM–Newton*	$3.4^{+0.3}_{-0.3}$	2.0×10^{44}	$1.43^{+0.11}_{-0.11}$
2013 02	2	*NuSTAR*	$1.7^{+0.1}_{-0.1}$	4.1×10^{44}	$1.47^{+0.13}_{-0.06}$

References: 1 – Young et al. (2002); 2 – Reynolds et al. (2015).

in the J, H, and K' bands (Canalizo et al. 2003). The authors determined that this same point source is also present in *Hubble Space Telescope* (*HST*) observations from 1996 and 1997. Based on the spectral energy distribution and the total luminosity, the most likely interpretation for this point source is that it is a tidally stripped galaxy core, that is in the process of merging with the giant elliptical galaxy. This supports the secondary black hole hypothesis put forth by Perley et al. (2017). Alternatively, the point source as seen by *Keck* and *HST* could represent the light from the secondary black hole itself.

Between 1 and 3 arcsec north-west and south-east of the AGN, a bipolar region with narrow emission lines was observed with the Wide Field and Planetary Camera II on board the *HST* (Tadhunter, Metz & Robinson 1994; Jackson, Tadhunter & Sparks 1998). The regions have an approximately paraboloidical shape and are oriented around the jet axis, suggesting that they scatter the light of the obscured AGN into our line of sight.

The nuclear region of Cygnus A has been studied at X-ray wavelengths as well, although these observations are more limited in their angular resolution. In *Chandra* ACIS observations, the AGN is moderately piled up with the standard 3.2s frame time. One 0.4s frame time observation from May 2000 has previously been used by Young et al. (2002) to study the region. At energies below 2 keV, the same bipolar emission regions are observed as with *HST*, while at energies above 2 keV, the AGN itself becomes visible.

In 2013, the *Nuclear Spectroscopic Telescope Array* (*NuSTAR*; Harrison et al. 2013) provided a new view of the AGN of Cygnus A at energies up to 70 keV. Reynolds et al. (2015) have compared this observation with an *XMM–Newton* observation from 2005. The two observations differ in two notable ways. First, the 2–10 keV X-ray luminosity appears to have doubled between 2005 and 2013. Secondly, subtle redshifted emission and blueshifted absorption features were detected around the iron K α line at 6 keV in the *NuSTAR* spectrum. These features are well fit by a fast, highly ionized wind with a high column density. This wind would presumably have started up in the 7 yr between the two observations. We have summarized the observed properties of the X-ray emission of the AGN as measured by *Chandra*, *XMM–Newton*, and *NuSTAR* in Table 1.

In this paper, we have searched for evidence of X-ray emission from Cygnus A-2, with the aim of shedding more light on the nature of this transient. Of particular interest are *Chandra* ACIS observations from 2000, 2005, and 2015–2017: first, because its angular resolution of 0.5 arcsec is only slightly larger than the 0.42 arcsec separation between the AGN and Cygnus A-2, and secondly because the 2015–2017 observations are from the same epoch as the original discovery of Cygnus A-2 with the VLA. We compare our results with *XMM–Newton* and *NuSTAR* observations, described in Reynolds et al. (2015), as well as archival observations from the X-ray Telescope (XRT) on board the Neil Gehrels Swift Observatory (hereafter referred to as *Swift*, Gehrels et al. 2004; Burrows et al. 2005).

We give an overview of the *Chandra* observations in Section 2. In Section 3, we image the soft X-ray emission and hard X-ray point source, compare the *Chandra* image data with MARX simulations, and use the image and the simulated data to look for an X-ray counterpart to Cygnus A-2. In Section 4, we perform an X-ray spectral analysis of the AGN with the *Chandra* data, including modelling the pile-up. We compare the 2–10 keV luminosities with *Swift* XRT, *XMM–Newton*, *NuSTAR*, *EXOSAT*, and *ASCA* (Advanced Satellite for Cosmology and Astrophysics) observations to construct a light curve of the AGN between 2000 and 2017. We also look for signatures of the fast, ionized wind in the *Chandra* data. We discuss the results of the image and spectral analysis in Section 5, and conclude in Section 6.

Throughout this paper, we have adopted a standard cosmology with $H_0 = 69.3$ km s^{-1} Mpc^{-1}, $\Omega_{\mathrm{M}} = 0.288$, and $\Omega_\Lambda = 0.712$ (Hinshaw et al. 2013). We use a redshift value of z = 0.0561 (Stockton, Ridgway & Lilly 1994). Using this cosmology, the linear scale is 66 kpc per arcminute and the luminosity distance $D_L = 253.2$ Mpc for Cygnus A. To facilitate comparison, X-ray luminosities cited from previous work have been re-calculated for this luminosity distance.

2 OBSERVATIONS

More than 2.2 Ms of *Chandra* ACIS data is currently publicly available on the *Chandra* Data Archive. However, a significant fraction of this data is pointed at some of the extended features in the system, such as the eastern and western hot spots, the merger region, and the north-western subcluster CygNW.

To minimize the size of the point spread function (PSF), we have selected only those observations pointed at the AGN. This leaves us with a total of 873ks of data. Of those 873ks, 43.9ks were taken in 2000 May, the first year of *Chandra* operations. ObsID 1707 is of particular note, because it is the only one with a short frame time of 0.4s, specifically chosen to avoid pile-up in the AGN. A second set of observations were taken in 2005, totalling 197.5ks. Finally, a large set of observations of were taken between 2015 October and 2017 May, totalling 595.6ks. We show a list of all the observations in Table 2.

Each of these data sets has been reprocessed using CIAO 4.9 and CALDB 4.7.4 (Fruscione et al. 2006). *Chandra's* pointing inaccuracy means that there can be an offset of up to an arcsec from the real coordinates. Therefore, an astrometric correction is necessary to compare the same region between *Chandra* data sets. We have followed procedure of Snios et al. (2018), briefly outlined here. ObsID 5831 was chosen as the reference observation, because of the long exposure time and the high number of events. We calculated the coordinates of the centre of mass within a 5 arcsec x 5 arcsec square, centred on the AGN. We then reprojected these coordinates to the astrometric position of the nucleus, $\alpha_{\mathrm{nuc}} = 19{:}59{:}28.35648$, $\delta_{\mathrm{nuc}} = +\,40{:}44{:}02.0963$ (Gordon et al. 2016) with *wcs_update*. We then cut out a 160 arcsec x 120 arcsec rectangular region of the central AGN of CygA. The event lists of the other ObsIDs were reprojected on to the sky frame of ObsID 5831. A 0.5–7.0 keV image of the reprojected events was then cross-correlated with that of ObsID 5831, and then fitted with a Lorentzian function, to determine the coordinate offset. This coordinate shift was then applied to the event list and the aspect solution file with *wcs_update*.

After the astrometric correction, we applied the following CIAO processing tools. For each ObsID, a new badpix file was built with *acis_build_badpix*. We applied this badpix file, and the latest gain and CTI corrections with *acis_process_events*. We created a new

Downloaded from https://academic.oup.com/mnras/article-abstract/486/3/3388/5470967 by Universiteit van Amsterdam user on 13 March 2020

Table 2. Overview of *Chandra* ACIS observations with the AGN close to the aimpoint. ObsIDs 360 and 1707 were taken with the ACIS-S array, all others with ACIS-I. The spectra and images of ObsIDs between dashed lines are considered to be within the same time period and are analysed together. ObsID 1707 is marked with an asterisk to indicate that it is the only short (0.4 s) frame time observation.

Date UTC)	Observation ID	Exposure (ks)
2000-05-21T03:13	360	34.7
2000-05-26T12:28	1707∗	9.2
2005-02-15T15:26	6225	24.3
2005-02-16T13:01	5831	50.8
2005-02-19T05:10	6226	23.7
2005-02-21T03:06	6250	7.0
2005-02-22T11:59	5830	23.2
2005-02-23T11:52	6229	22.8
2005-02-25T04:27	6228	16.0
2005-09-07T04:48	6252	29.7
2015-10-28T11:49	17508	14.9
2015-11-01T16:48	18688	34.6
2016-06-13T21:02	18871	21.8
2016-06-18T17:52	17133	30.2
2016-06-26T16:13	17510	37.3
2016-07-10T22:52	17509	51.2
2016-08-15T22:10	17513	49.1
2016-09-15T05:46	17512	66.9
2016-11-12T12:56	17507	32.4
2016-12-13T10:56	17514	49.4
2017-01-20T18:09	17135	19.8
2017-01-26T00:42	17136	22.2
2017-01-28T14:24	19996	28.6
2017-02-12T05:40	19989	41.5
2017-05-10T02:01	17511	15.9
2017-05-13T21:25	20077	27.7
2017-05-20T23:24	17134	29.4
2017-05-21T17:12	20079	23.8
	Total	837

level 2 event file by filtering for good grades (0,2,3,4,6). After that, we filtered for GTIs with the *deflare* procedure.

3 SOURCE IMAGING AND THE PSF

3.1 Imaging

We imaged the central region of Cygnus A in three different energy bands: the soft (0.5–1.275 keV), intermediate (1.275–2.2 keV) and hard (2.2–8.0 keV) bands, chosen after Young et al. (2002). The ACIS blank-sky backgrounds were used as backgrounds for these images. These backgrounds are imported from CALDB with the *acis_bkgrnd_lookup*, and scaled to the event files by using the counts between 10.0 and 12.0 keV. The event files and backgrounds were then reprojected to the common tangent point of ObsID 360.

For each ObsID, we extracted a spectrum from a region with a radius of 6 arcsec, centered on the source. We then fit a model to them to obtain energy weightings for the exposure maps. These fits are not meant to find the physical characteristics of the source, but only to find a model curve that approximates the spectral shape, to obtain a rough energy weighting for the exposure-corrected images. To the 0.5–2.2 keV band, we fit a power law multiplied by the galactic absorption component, which we froze at 3.1×10^{21} $N_{\rm H}$ cm^{-2} (Dickey & Lockman 1990). To the 2.2–8.0 keV band, we fit the same model, but we leave the absorption component as a free parameter, as the hard X-rays come from the highly absorbed central source (Young et al. 2002).

These model curves were used to obtain spectral weightings, and we used these to create instrument maps and exposure maps with the tools *mkinstmap* and *mkexpmap*. The exposure maps were then reprojected to the tangent point of ObsID 360.

We binned each event file and blank-sky background into the 3 energy bands, for each of the 3 time bins of 2000, 2005, and 2015-2017. We then sliced a 12.5 x 12.5" image of the central region for each ObsID, spatially binned at 0.2 native pixel resolution. We used *dmregrid* to bin the exposure maps to the same resolution. We subtracted the backgrounds from the data and divided by the exposure map to obtain images of the central region. The images are shown in Fig. 1.

The nucleus, visible in the 2.2–8.0 keV band, has an irregular, non-pointlike shape in the 2000 and 2005 observations. These asymmetries are the strongest in the 2005 observations, and they show up in all of the individual ObsIDs from 2005, indicating they are not astrometry related. Further inspection of these observations shows that they were carried out with a large SIM_Z offset, about 10 mm larger than the nominal value. At an off-nominal offset, the curved detector focal place intersects the focal surface of the mirrors differently, causing a different defocus. We believe this to be responsible for the irregular PSF shape in the 2000 and 2005 observations.

3.2 Simulations and the pile-up fraction

We have used the simulation tool MARX (Davis et al. 2012) to simulate the spatial and spectral distributions of events for each observation. The purpose was to determine the size of the region in which pile-up affects the spectrum and to be able to compare the image to data, to look for evidence of any hard X-ray emission that is more extended than the point source.

As discussed in Section 3.1, the 2000 and 2005 observations show an unusual PSF shape, with wings to the north, south, east, and west. We have not been successful in reproducing this irregular PSF shape with MARX. In this section, we therefore focus on the 2015–2017 observations, totalling around 595.6 ks of data. As these observations were taken shortly after the discovery of Cygnus A-2, these are the most likely to show any X-ray emission from the transient.

Based on the images of the source, it is apparent that the soft X-rays primarily come from an extended region, while the hard X-rays primarily come from the point source. If pile-up was not a factor, the hard X-rays could be simulated as a point source and the soft X-rays could be ignored. However, because of pile-up, both the spatial and spectral distribution of the source emission affect the spectrum extracted from a region. Thus, the soft X-ray photons coming from the extended region need to be taken into account when simulating the source. We therefore performed two separate simulations for each ObsID. The soft, extended emission between 0.5 and 2.2 keV was simulated by using the exposure-corrected image of the source (`SourceType = IMAGE`), and an extracted spectrum, both obtained from ObsID 1707 and filtered for counts between 0.5 and 2.2 keV. MARX matches the brightness distribution of the simulated source to the input image, so that the simulated source has the same shape, and the same spectral distribution. The 2.2–8.0 keV emission was simulated as a point source (`SourceType = POINT`). The input spectrum was again obtained from ObsID 1707, filtered for counts between 2.2 and 8.0 keV.

Downloaded from https://academic.oup.com/mnras/article-abstract/486/3/3388/5470967 by Universiteit van Amsterdam user on 13 March 2020

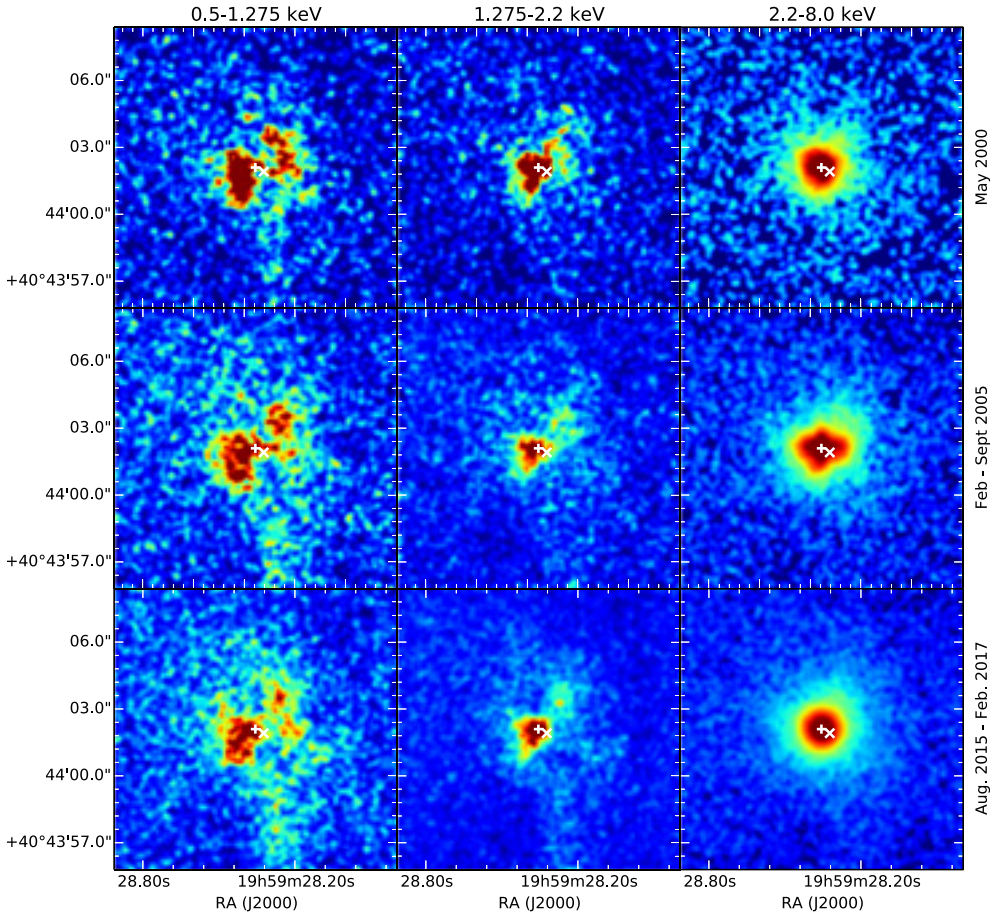

Figure 1. 12.5 arcsec x 12.5 arcsec images showing the central region flux over time. The image has been binned at 0.2 ACIS pixel size in both dimensions, and smoothed by a 0.5 arcsec full width at half-maximum Gaussian. The astrometric positions of the AGN and Cygnus A-2 are, respectively, indicated by a cross and an X.

Other parameters relevant for the simulation, like the aspect solution file, the exposure time, detector type, and SIM offsets, were all used in the simulation by reading the header of each event file. The AspectBlur parameter, which blurs the PSF by a fraction of an arcsecond to account for the uncertainty in the determination of the aspect solution, was set to 0.20 arcsec. This is the recommended value for ACIS-I.

After both simulations were performed for a given ObsID, the simulations were combined with the tool *marxcat*. We then applied the pile-up tool *marxpileup* to the combined simulation and binned images of the same size as the data, a 12.5 x 12.5 arcsec image at 0.2 native pixel resolution. Finally, we filtered each simulated observation for events between 2.2 and 8.0 keV, and summed all the images of individual observations to obtain the combined 2.2–8.0 keV simulated data of the 2015–2017 observations. Because the source is embedded in the intracluster medium (ICM), there are a significant number of background counts, especially at radii beyond 3 arcsec. Therefore, we modelled the background as a linear function $bkg(r) = a*r + b$ that is fit to the data – model residual.

The results of our comparison between data and the simulation are shown in Fig. 2. We note that, to achieve the best match between the data and the simulation, we iterated over the SourceFlux parameter, which renormalizes the total flux of the model. Because the soft X-ray emission is a few kiloparsec in size, we do not expect that it

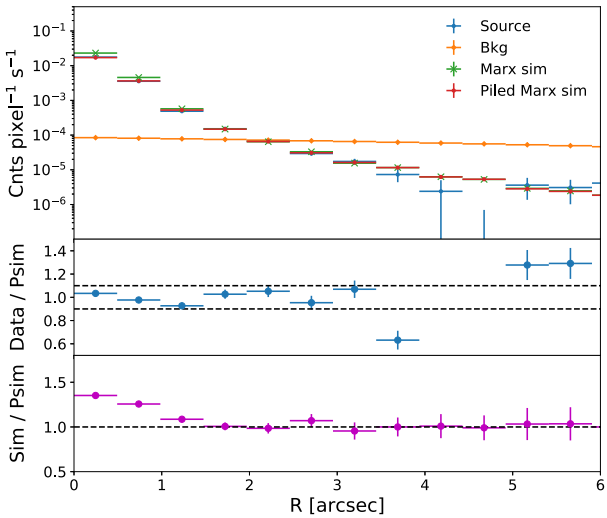

Figure 2. *Top:* Surface brightness profile of the composite 2015–2017 2.2–8.0 keV data in blue, the background in yellow, and the simulated source (green) and piled simulated source (red), made with MARX. *Middle:* Residual of the data divided by the piled simulation. *Bottom:* The ratio between the unpiled and piled simulations.

Downloaded from https://academic.oup.com/mnras/article-abstract/486/3/3388/5470967 by Universiteit van Amsterdam user on 13 March 2020

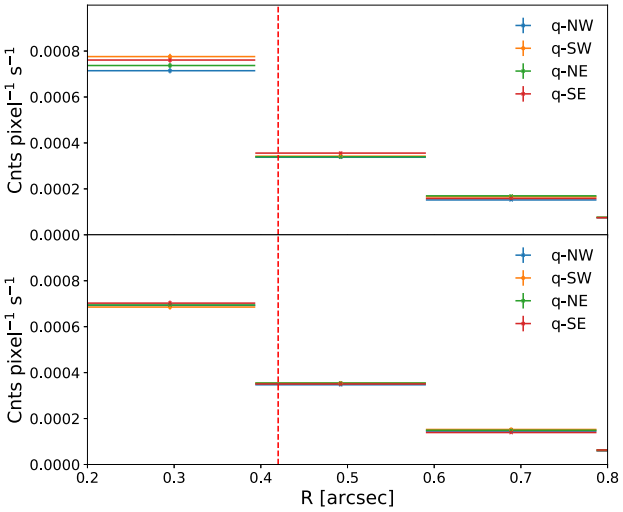

Figure 3. *Top:* Counts per pixel profiles of the 2015–2017 data, divided in NW, NE, SW, and SE quadrants. The dashed red line indicates the location of Cygnus A-2, at 0.42 arcsec, in the SW quarter. *Bottom:* As above, but for the image simulated with MARX.

varied significantly between 2000 and 2015, and so we leave this input spectrum as it is. However, the AGN itself could well have changed in brightness. We iterated several times to find the best match between the piled PSF and the image data, and ultimately found the best match by setting the SourceFlux to about 90 per cent of that of the input spectrum of ObsID 1707. In Section 4.1, we compare this estimate against the luminosities from the spectral analysis.

In the bottom panel of Fig. 2, we have compared the PSF and the piled PSF to determine the radius within which pile-up is significant, approximately 1.3–1.5 arcsec. Furthermore, we determine that the piled PSF contains 78 per cent of the counts of the unpiled PSF, yielding a pile-up fraction of 22 per cent. This provides us with an estimate of the pile-up fraction to compare against in Section 4.1.

3.3 Searching for an X-ray counterpart to Cygnus A-2

We have used the 2015–2017 data to search for evidence of Cygnus A-2. In the 2000 and 2005 observations, the irregular shape of the PSF makes this comparison more difficult, as we were not able to reproduce the shape in the MARX simulations. The 2015-2017 data is the most obvious place to look for Cygnus A-2 in either case, because it is the time period closest to detection. If Cygnus A-2 is emitting X-rays, it would elongate the circular shape of the point source. We therefore look for hints of an elongated point source, by comparing the 2.2–8.0 keV image data from Section 3.1 with the simulated image from Section 3.2.

In the 2015–2017 image, we determined the centre coordinate by calculating the centre of mass of the image. We then divided the image into quadrants NW, NE, SW, and SE, using the centre of mass as the centre point. The transient is located at 0.42 arcsec south-west of the centre, and would thus be expected to show most clearly in the SW quadrant. We calculated the SB profile for each of the quadrants. We did the same for the simulated and piled PSF in order to understand the order of magnitude of asymmetries in the PSF versus the image. We show the SB profiles of the quadrants of both the image and the PSF in Fig. 3.

While the SE quadrant has the highest surface brightness at 0.42 arcsec, the SW has the same surface brightness to within just a few per cent. In the simulated PSF, we see similar kinds of deviation, although slightly smaller than in the data. Around 0.4 arcsec, the differences are of order 1–2 per cent. It is likely that at least some of these differences are caused by the fact that the centre of the source is not perfectly in the centre of a single subpixel, which means the different quadrants are not perfect quarters of the circle. In the range from 0.2 to 0.6 arcsec, the total counts difference between the SW and NE quadrants in the data is about 5 per cent. We therefore expect the maximum observed 2.2–8.0 keV flux to be not more than 5 per cent of that of the AGN.

As support for this estimate, we revisited the `marx` simulations of Section 3.2. We created a new simulated image by adding a secondary point source at the location of Cygnus A-2 to the `marx` simulations, and scaled the input spectrum of that point source to 5 per cent of the primary point source spectrum. We then created two residual images: the first one by dividing the 2015–2017 2.2–8.0 keV data by the original simulated image, and the second one by dividing the data by the simulated image with the transient added. The left-hand and right-hand panels of Fig. 4 show these two residual images. The left-hand panel shows a similar structure to the surface brightness profiles in Fig. 2: a decent match up to a radius of 2.5–3 arcsec. At larger radii, the background dominates. The residual appears to be roughly radially symmetric. The right-hand panel of Fig. 2 shows the data divided by the simulated image with the transient added. In this residual, there is a visible deficit at the location of the secondary point source, particularly noticeable towards the south-west. We conclude that a source with a flux more than 5 per cent would have been visible in the comparison between the data and the MARX simulations.

4 SPECTRAL ANALYSIS

4.1 *Chandra* observations

We have defined a circular extraction region with a radius of 3 arcsec, centred on the AGN. As a local background, we used an annulus around the source between 6 and 10 arcsec. The source and background regions, as well as the response files, were extracted from each ObsID with the CIAO tool *specextract*. All observations in 2005 and between 2015 and 2017 were combined with *combine_spectra*. The 2005 and 2015–2017 observations were all taken with the ACIS-I detector, and thus we did not have to worry about different detector types. After extracting, we fit the spectra with the CIAO fitting and modelling tool `sherpa` (Freeman, Doe & Siemiginowska 2001).

As previously mentioned, ObsID 1707 is unique because it is the only short frame time observation of the AGN, and therefore is not piled up. For ease of reference, we will refer to ObsID 1707 as the 2000 SF (short frame time) observation, and to ObsID 360 as the 2000 NF (normal frame time) observation. As our analysis in Section 3.2 has shown, there is moderate to strong pile-up in this source that needs to be accounted for in the spectra of the normal frame time observations. To this end, we have used the pile-up model `jdpileup` (Davis 2001).

Several parameters are used in `jdpileup` to parametrize the amount of pile-up in the spectrum. The most important of these are (1) n, describing the number of 3x3 islands in which pile-up is applicable, (2) f, the fraction of the total flux of the spectrum that is inside the pile-up region, and (3) α, a parametrization of grade migration, where if N photons are piled together, the chance that

Downloaded from https://academic.oup.com/mnras/article-abstract/486/3/3388/5470967 by Universiteit van Amsterdam user on 13 March 2020

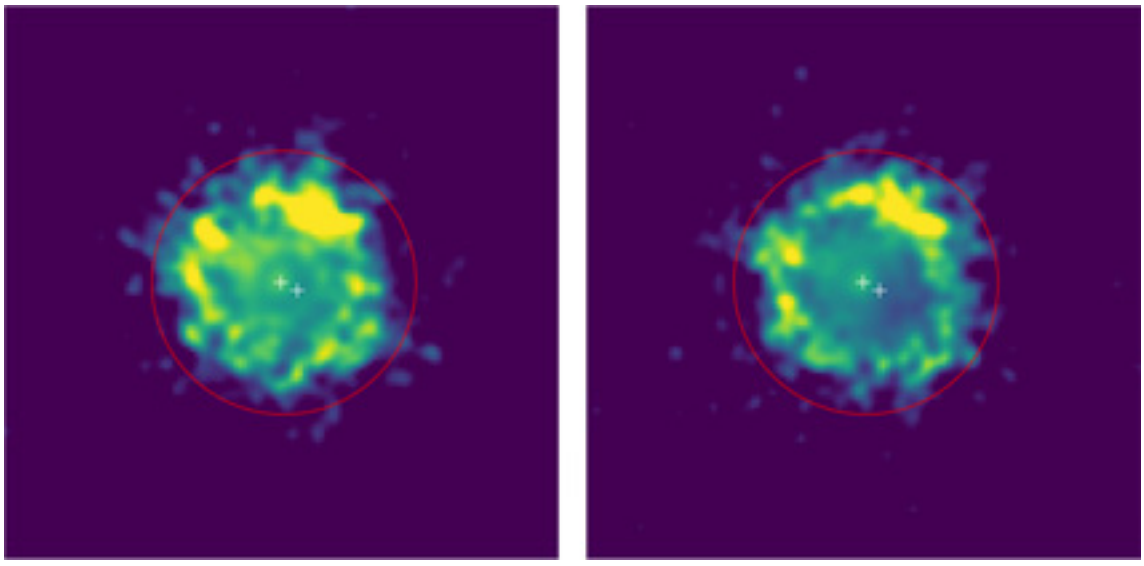

Figure 4. *Left:* Residual of the 2.2–8.0 keV image divided by the simulated image. *Right:* Residual of the 2.2–8.0 keV image divided by the simulated image with an additional point source, with 5 per cent the flux of the AGN point source, at the location of Cygnus A-2. Both images have been smoothed by a 0.5 arcsec Gaussian. The white crosses indicate the astrometric locations of Cyg A and Cyg A-2, the red circle indicates a radius of 3 arcsec.

they are registered as a single photon with their combined energy is given as α^{N-1}.

The PSF simulations from the previous section have shown that pile-up significantly affects the data up to about 1.3 arcsec radius. We estimate the parameter f from the 2.2–8.0 keV flux image of the 2000 SF observation. We calculate the flux ratio of the flux within the estimated pile-up radius of 1.3 arcsec, and 3 arcsec, the total size of the extraction region. From the image we measure $f = 0.93$. Although the PSF is a bit more extended in 2005 compared to 2000, we assume this will not significantly alter the value of f and we have chosen to leave this parameter fixed.

The parameter n represents the number of 3x3 pixel islands in the observation where pile-up is significant. After the example in Davis (2001), we have counted the number of full pixels in a 1.3 arcsec circle and divided this number by 9. We count 14 pixels, and therefore we set $n = 1.55$.

Next, we consider the spectral model. Previous modelling of the AGN by Young et al. (2002) and Reynolds et al. (2015) shows that the AGN spectrum is a heavily absorbed power law. Because of the heavy absorption, there are virtually no counts coming from the AGN below 2 keV. On top of the power law, there is a fluorescent iron-K α emission line in the spectrum, around 6.4 keV rest-frame energy. This line can be modelled either with a Gaussian or with a more detailed Compton-thick reflection model. While the reflection model is the more physical of the two, it is difficult to fit this to the *Chandra* data, where we are restricted to the 0.5–7.0 keV energy range, below most of the Compton reflection features. In fact, Reynolds et al. (2015) have attempted to fit the reflection model to the *XMM–Newton* data and find that the reflection model does not significantly improve the fit over a Gaussian emission line. We therefore use a Gaussian to describe the fluorescent emission line. Beyond the iron-K α line, Young et al. (2002) note the presence of an absorption edge at a rest-frame energy of around 7.2 keV or 6.8 keV observed energy. We therefore include this component in our model, and we have fixed the threshold energy of the absorption edge to 6.8 keV.

The presence of pile-up in the spectrum means that we must consider the full *Chandra* ACIS energy range, and not just photons above 2 keV, where the AGN is bright. This is because the soft X-ray photons will affect higher energies by becoming piled. This presents a problem, as the soft X-ray photons come from an extended region rather than the AGN. Therefore, the parameters of the pile-up model are not necessarily valid. We have attempted to circumvent this problem by including the model components of the soft X-ray emission in the total model, but *not* fitting the data below 3 keV. The soft X-ray emission is modelled as a second, unabsorbed power law as well as three fluorescent emission lines, modelled with Gaussians (see Young et al. 2002). Given that this model is not fit to the data, we do not consider the fit values that we obtain for the soft X-ray model components as physically accurate. Rather, the soft X-ray model components exist purely to model how the soft X-ray band of the spectrum affects the shape of the spectrum in the hard X-ray band due to pile-up. During the fitting process, we have tweaked the parameters of the soft X-ray model components, in particular the amplitude of the emission lines, such that they do not deviate too far from the soft X-ray data.

Lastly, we take into account the contribution of the thermal ICM. We have modelled the ICM with a thermal `APEC` model, absorbed by the galactic absorption. We fit this model to the background annulus between 0.5 and 4 keV. At energies beyond 4 keV, the PSF of the AGN is so wide that the hard X-ray photons from the AGN significantly contribute to the background annulus. For each time period, we determine the abundance and temperature with a fit to the background annulus. We then freeze the temperature and abundance in the fit to the source spectrum, allowing only the normalization to vary. The temperature and abundance are slightly different between 2000 and the later time periods. This can be explained by the fact that the 2000 observations were taken with ACIS-S and the later observations with ACIS-I. The changes are of order 5–10 per cent, and the ICM temperature and abundance for all spectra are around $kT = 3.5$ keV and $Z = 0.55\ Z_{\odot}$.

The final model is then as follows: `ABS1 * (ICM + POW1 + 3*emLINES + ABS2 * EDGE * (POW2 + emLINE))`.

Downloaded from https://academic.oup.com/mnras/article-abstract/486/3/3388/5470967 by Universiteit van Amsterdam user on 13 March 2020

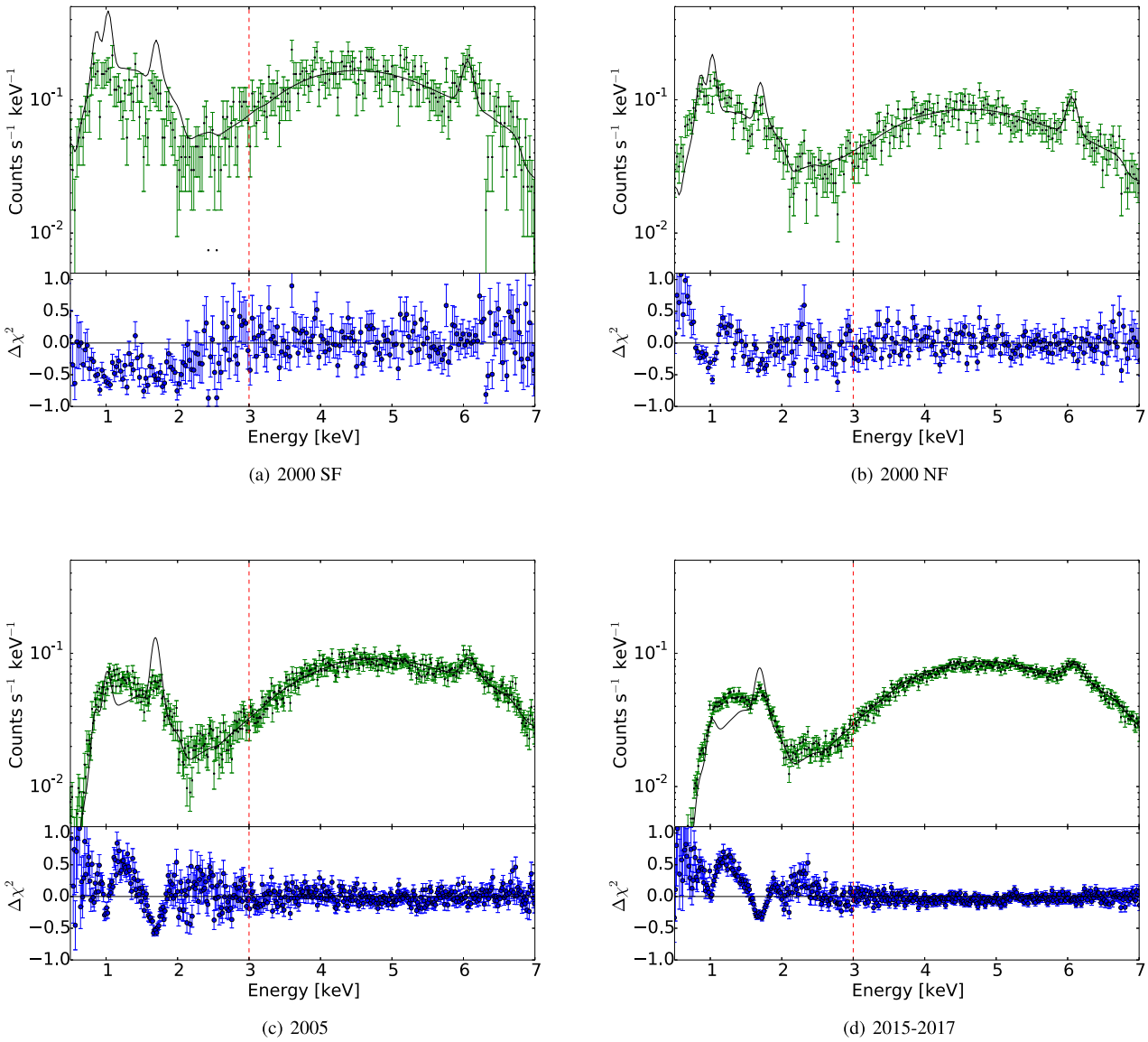

(a) 2000 SF (b) 2000 NF

(c) 2005 (d) 2015-2017

Figure 5. The spectral fits to the 2000 short and normal frame time, 2005 and 2015–2017 observations. Only energies above the red line at 3 keV are included in the fit.

This model is used as input to the `jdpileup` model for all spectra except the 2000 SF observation. The galactic absorption is set to 3.1×10^{21} cm^{-2} (Dickey & Lockman 1990). The full width at half-maximum (FWHM) of each emission line is set to 0.07 keV, roughly the expected FWHM of *Chandra*. We took the energies of the soft X-ray emission lines from Young et al. (2002), and left the energy of the iron-K α emission line as a free parameter. We have also linked the photon index of POW1 to the photon index of POW2, which is what is expected if the soft X-ray emission is scattered AGN light.

We have fit the 2000 SF and 2000 NF spectra simultaneously. Because these were taken days apart, we have assumed that parameters such as the photon index and the absorbing column have stayed the same in this time period. Simultaneously, fitting the same model to these two spectra helps to further constrain the pile-up model. The 2005 and 2015–2017 spectra were fit separately, giving us four spectra and three time periods in total.

Our best fits to the spectra are shown in Fig. 5, and the results of those fits are given in Table 3. During the fitting process we noticed that the grade migration parameter α, when left as a free parameter, takes on a value of 1 when fitting the 2005 and 2015–2017 spectra. Because more grade migration hardens the spectrum, it is likely that there is some degeneracy between α and the photon index Γ, which makes it difficult to find the appropriate value of α. In the 2000 spectra this degeneracy is easier to break, because the SF and NF spectra are fit simultaneously. We therefore fixed the grade migration parameter in these observations to 0.55, the value found from the fit to the 2000 observations.

Furthermore, there seems to be no significant change in the spectra between the three different time periods. The photon index is lower in the 2005 and 2015–2017 observations, but given the degeneracy between α and Γ, it is unclear whether this is a real trend. The photon indices we find are also broadly consistent with the photon index $\Gamma = 1.43 \pm 0.11$ that Reynolds et al. (2015) find for the *XMM–Newton* data, using the `ICM + cABS(PL`

Downloaded from https://academic.oup.com/mnras/article-abstract/486/3/3388/5470967 by Universiteit van Amsterdam user on 13 March 2020

Table 3. Results of our fits to the 2000, 2005, and 2015–2017 *Chandra* ACIS spectra with the source model described in the text. Parameters directly obtained from the fit are shown with the 90 per cent confidence interval.

Year	α^a	$f_{\text{pile-up}}{}^b$	$N_H{}^c$ (10^{22} cm^{-2})	Γ	$L_{2-10\,\text{keV}}$ (10^{44} erg s^{-1})	$\mu_{\text{iron-K}\,\alpha}{}^d$ (keV)	$\text{EW}_{\text{iron-K}\,\alpha}{}^e$ (eV)	$\tau_{\text{edge}}{}^f$	χ^2
2000	0.55 ± 0.05	0.19	19.2 ± 4.3	1.42 ± 0.12	2.0 ± 0.2	6.40 ± 0.01	219	0.32 ± 0.15	330/320
2005	0.55[h]	0.19	19.1 ± 3.9	1.30 ± 0.04	2.2 ± 0.2	6.43 ± 0.01	149	0.40 ± 0.23	335/321
2015–2017	0.55[h]	0.17	20.7 ± 3.3	1.23 ± 0.04	1.9 ± 0.2	6.44 ± 0.01	150	0.35 ± 0.10	412/383

[a]The grade migration parameter.
[b]The fraction of piled events.
[c]The column density to the nucleus.
[d]The median rest-frame energy of the iron–K α line.
[e]The equivalent width of the iron–K α line.
[f]The optical depth of the absorption edge at rest-frame energy 7.2 keV.
[h]This parameter was fixed, see the text for details.

+ emLINE) model. The photon index is found to be higher, around 1.60, in the *NuSTAR* data, but this is somewhat model dependent. In particular, adding reflection and wind model components changes the way the region around the iron–K α line and beyond is modelled, and this can shift the photon index of the entire spectrum.

One particular challenge of pile-up models is that it can be difficult to distinguish between a source with a high flux/high pile-up fraction, and low flux/low pile-up fraction. For each of the fits, we have calculated the pile-up fraction in sherpa with the command *print(get_pileup_model())*. The pile-up fraction for all observations is between 0.17 and 0.19, comparable to the pile-up fraction of 0.22 found in Section 3.2. Additionally, the luminosity in 2015–2017 is about 95 per cent of the 2000 luminosity, consistent with the 90 per cent estimate we used to simulate the data with marx.

We have used the sherpa tool *sample_flux* to estimate the 90 per cent confidence interval on the AGN luminosity. We find that for all time periods, the error is on the order 10 per cent.

The *XMM–Newton* data has significantly higher absorbing column (3.0×10^{23} cm^{-2}) than the *Chandra* observations from 2005. Because these observations were taken close together in time, we would expect the absorbing column to be roughly the same value. We tried to re-fit the 2005 *Chandra* spectrum by fixing the absorbing column to the *XMM–Newton* value, but were unable to find a good fit with this constraint. Most of *Chandra* exposures in 2005 were taken in February, with only ObsID 6252 being taken later, in September. This is also the ObsID that is closest in time to the *XMM–Newton* observation date in October. To see whether the absorbing column changed between February and September, we fit the spectral model to ObsID 6252 separately to look for signs of a higher absorbing column. However, we find a value that is consistent with that of the total 2005 spectrum, $N_H = (17.6 \pm 2.2) \times 10^{22}$ cm^{-2}. We therefore find no indication in the *Chandra* data that the absorbing column increased towards the *XMM–Newton* observation date.

The intrinsic luminosity that we find from simultaneously fitting the 2000 SF and 2000 NF spectra is $L_{2-10\,\text{keV}} = 2.0 \times 10^{44}$ erg s^{-1}. This is consistent with the value of $L_{2-10\,\text{keV}} = 1.9 \times 10^{44}$ erg s^{-1} that Young et al. (2002) find, using the 2000 SF observation. Furthermore, the 2005 *Chandra* luminosity is consistent with the *XMM–Newton* luminosity.

4.2 *Swift* XRT observations

To be able to study the long-term behaviour of the nuclear region, we have searched for other X-ray observations of Cygnus A between 2000 and 2015. *Swift* XRT has observed Cygnus A eight times between 2006 January and 2013 March. Two observations, on 2013 February 17 and March 1, correspond exactly to *NuSTAR* observation dates. The full observation log is given in Table 4.

Table 4. The *Swift* XRT observations of the field of Cygnus A, in Photon Counting Mode. ObsIDs between dashed lines were combined.

Date UTC)	Observation ID	Exposure (ks)	Distance from centre (arcsec)
2006-01-23T05:08	00035024002	5.1	103
2007-03-06T04:26	00036397001	9.0	98
2007-03-08T00:57	00036397002	12.4	84
2008-08-23T15:08	00036397003	5.6	118
2008-08-27T04:19	00036397004	3.7	139
2013-02-17T20:08	00080235002	2.0	118
2013-02-27T23:58	00082067001	1.9	399
2013-03-01T16:01	00080235003	1.9	95

For each of these observations, obtained in Photon Counting Mode, we have created a spectrum and associated response files. This was done using HEASOFT version 6.24, and the associated CALDB for *Swift*. Because the FWHM of the XRT PSF is 18 arcsec, the AGN is not clearly resolved inside the larger Cygnus A X-ray environment. Therefore, any spectrum extracted from the Cygnus A region is significantly contaminated by emission from the surrounding ICM, which is relatively hot and bright. This is, in principle, not different from *NuSTAR*, but there are additional problems for *Swift* XRT: the count rate of the observations, around 0.56 counts s^{-1}, is above the approximate pile-up threshold count rate of 0.5 counts s^{-1}.[1] The data are therefore likely piled up. Additionally, *Swift* is more sensitive to soft X-ray photons than *NuSTAR*, which means the contribution of the ICM to the spectrum is stronger.

While the *Swift* software has tools to correct for pile-up by excising the center pixels of the observation, these tools assume that the extracted region is a point source on a constant background. Because of the ICM that the AGN is embedded in, this is not the case here and therefore any pile-up correction will be inaccurate.

To minimize ICM contamination, we chose a relatively small extraction circle of 18 arcsec, centred on the brightest pixel of each ObsID. We combined the spectra from two ObsIDs in 2007 March, two in 2008 August, and three in 2013 February/March. Together with the 2006 data point, this makes four data points in total.

[1]http://www.swift.ac.uk/analysis/xrt/pileup.php

Downloaded from https://academic.oup.com/mnras/article-abstract/486/3/3388/5470967 by Universiteit van Amsterdam user on 13 March 2020

All of the *Swift* spectra have a strong peak in the soft X-ray band, between 0.5 and 4 keV, and a peak in the hard X-ray band, between 4 and 10 keV. We interpreted the soft X-ray peak to be the ICM and have therefore excluded energies below 4 keV, where the ICM is the brightest. We fit an observed power law to the spectrum between 4 and 10 keV and use that to determine the observed luminosity. We note that, given the presence of pile-up, and the potentially still significant presence of contaminating ICM, we do not regard the obtained fit values for the photon index and the absorbing column as physically accurate. Instead, the model serves as a way to determine the observed, rather than the intrinsic, luminosity from the spectra.

After obtaining the observed luminosities, we estimated the intrinsic luminosities by applying a few different corrections. First, we applied a pile-up correction. Because the count rate is slightly above the pile-up count rate threshold, we assume a small pile-up fraction of 10 per cent. This rough estimate is based on the fact that the count rate in our *Swift* spectra, 0.56 counts s^{-1}, is roughly 10 per cent higher than the pile-up treshold count rate, 0.5 counts s^{-1}. Secondly, we estimated the ICM contribution by fitting an absorbed thermal model to the spectra between 0.5 and 2.0 keV, and calculating the luminosity of this thermal model between 4 and 10 keV. The estimated 4 and 10 keV ICM luminosity within the extraction region is $\sim 2.5 \times 10^{43}$ erg s^{-1}. We subtracted this from the pile-up-corrected observed luminosity. Thirdly, we increased the luminosity by 5 per cent to account for the difference between the 2–10 keV and 4–10 keV band. Finally, we de-absorbed the luminosities, by assuming a photon index $\Gamma = 1.4$. In the 2006 and 2013 observations, we assumed the absorbing column to be the same as in the 2005 *Chandra* and 2013 *NuSTAR* observations, respectively. In the 2007 and 2008 observations, we assumed a range in absorbing column between 1 and 3×10^{23} cm^{-2}, which adds an uncertainty of 40 per cent to the calculated intrinsic luminosity.

4.3 X-ray observations before 2000

To measure the long-term X-ray behaviour of Cygnus A, we searched the literature for X-ray observations before 2000. Cygnus A has been observed by several X-ray telescopes before *Chandra*, although in these observations, the AGN was not spatially resolved from the ICM. Given the lower spatial and spectral resolution of these instruments, and the relative brightness of the ICM, the measured intrinsic AGN luminosities are a lot more uncertain.

Cygnus A was observed with the European X-ray Observatory Satellite (*EXOSAT*) in 1985 (Arnaud et al. 1987). A fit to the data with a thermal component and an absorbed power law yielded an intrinsic 2–10 keV luminosity of 2.8×10^{44} erg s^{-1}, while the thermal component has a luminosity of 3.4×10^{44} erg s^{-1}.

In 1991, Cygnus A was observed with the *Ginga* satellite (Ueno et al. 1994). Like with the *EXOSAT* observations, the authors find that the best description of the data is provided by a model consisting of (1) a thermal and (2) an absorbed power-law component. The intrinsic luminosity was found to be much higher than during the EXOSAT observation, about 5.5×10^{44} erg s^{-1}, and a thermal luminosity of 5.8×10^{44} erg s^{-1}. However, the Large Area Counter instrument on board *Ginga* that was used to observe Cygnus A has a PSF with a FWHM of 1.1 deg × 2.0 deg (Turner et al. 1989). With such a large field of view, it measures the spectrum of the entire cluster, and cannot be used to make a reliable measurement of the AGN luminosity. We therefore do not include the *Ginga* luminosity in our light curve.

Finally, Cygnus A was observed by the *ASCA* in 1993 May and October. The data were analysed by Sambruna, Eracleous & Mushotzky (1999). Fitting a thermal model plus absorbed power law to these data, they found that the nuclear flux increased by a factor of more than 3 in 5 months, while the absorbing column increased from 1.1×10^{23} to 1.5×10^{23} cm^{-2}. Because we were unable to reproduce the conversion from observed to intrinsic luminosity listed in that paper, we retrieved the archival data from the HEASARC data archive and re-analysed the spectra. We selected the pre-extracted spectrum of the entire field that is included in the standard data products, and used the spectra of the Solid State Imager (SIS) instrument in Bright mode.

Comparing *ASCA* observations, we find that the 2–10 keV count rate is about 10 per cent higher in October than in May. We freeze the photon index to 1.8, the value found by Sambruna et al. (1999), and leave the other parameters free. We fit the spectra between 3 and 9 keV and find intrinsic luminosities for the non-thermal component of 3.1×10^{44} and 3.0×10^{44} erg s^{-1} for May and October, respectively. Interestingly, the absorbing column is also much higher than what was found by Sambruna et al. (1999), 2.6×10^{23} and 3.1×10^{23} cm^{-2}, respectively. This is likely because we used 3 keV instead of 4 keV as a lower limit, which allows for a better restriction of the absorbing column.

4.4 The AGN light curve

We have combined all the available luminosity data on the AGN of Cygnus A into a single light curve in Fig. 6. Shown are the *Chandra* data from Section 4.1, the *Swift* data from Section 4.2, the *EXOSAT* and *ASCA* data from Section 4.3, and the *XMM–Newton* and *NuSTAR* data from Reynolds et al. (2015).

We note that the error bars on the luminosities are in some cases, rather uncertain. Uncertainty estimates on the luminosity are not reported for the *EXOSAT* data point in Arnaud et al. (1987) nor for the *XMM–Newton* and *NuSTAR* data points in Reynolds et al. (2015). For *EXOSAT*, we based our uncertainty estimate on the uncertainty in the absorbing column, as well as adding 25 per cent systematic uncertainty because of the fact that the AGN is not resolved within the larger environment, and the limitations of the simple two-component model that is fit to this data. For the *ASCA* data, which we have re-analysed in this work, we used the *sample_flux* tool in `sherpa` to obtain 90 per cent confidence intervals. For the *Chandra* data, we similarly used *sample_flux* to estimate the 90 per cent confidence interval. For the *XMM–Newton* and *NuSTAR* data, we based our estimate on uncertainty in the absorbing column as well as a 5 per cent systematic error. For *Swift* XRT, we based our estimate on the uncertainty in the absorbing column and a 25 per cent systematic error. The systematic error in the case of *Swift* is large because of the assumptions we had to make when converting observed luminosity to intrinsic luminosity.

Although there are some hints that the average luminosity was higher before 2000, this increase is not significant because of the large error bars on the *EXOSAT* and *ASCA* luminosities. All data points are consistent with a luminosity of 2×10^{44} erg s^{-1}, except for in 2013, when a statistically significant higher luminosity was observed by both *NuSTAR* and *Swift*. We discuss potential reasons for this increase in Sections 5.1 and 5.3.

4.5 Wind signatures in the *Chandra* data

Reynolds et al. (2015) previously detected a fast and ionized wind in the 2013 *NuSTAR* spectrum. The presence of this wind was deduced from a P Cygni-like spectroscopic feature around the iron–K α line: a redshifted emission component that moves the centroid of

Downloaded from https://academic.oup.com/mnras/article-abstract/486/3/3388/5470967 by Universiteit van Amsterdam user on 13 March 2020

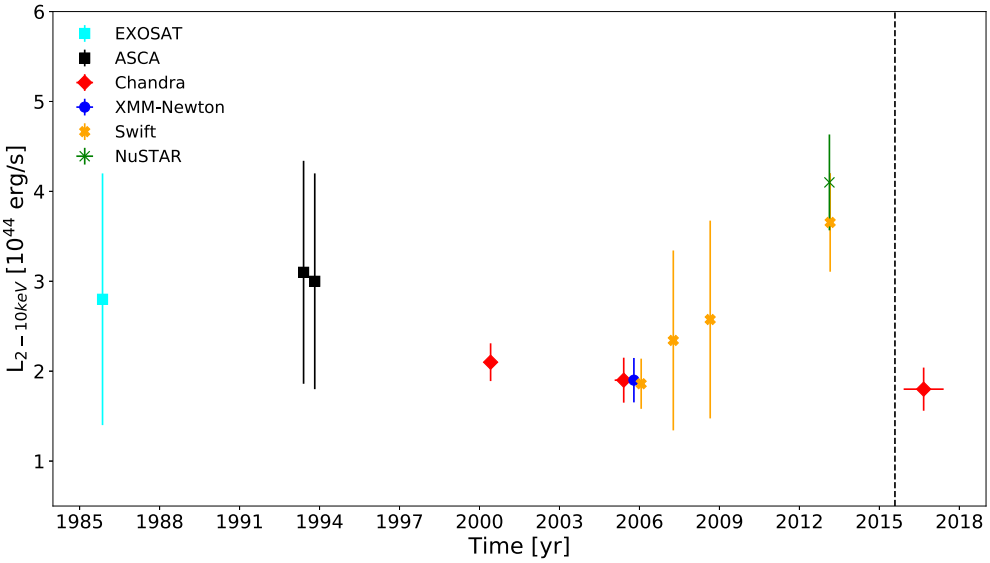

Figure 6. The intrinsic 2–10 keV luminosity of the AGN of Cygnus A over time, as measured by *EXOSAT*, *ASCA*, *Chandra*, *XMM–Newton*, *NuSTAR*, and *Swift*. The dashed line indicates the date of first discovery of Cygnus A-2 with the VLA.

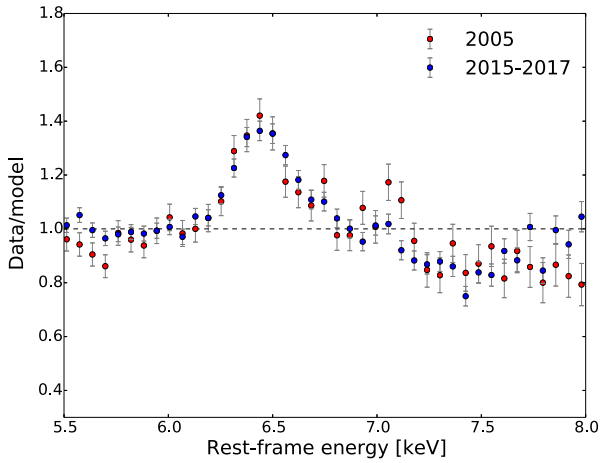

Figure 7. The *Chandra* ACIS 2005 and 2015–2017 ratio spectra. The horizontal axis shows the Cygnus A rest-frame energy. The data have been divided by a piled, absorbed power law, leaving the iron–K line and the absorption edge at 7.2 keV.

the iron–K α line to lower energies, and a blueshifted absorption component of the power-law continuum. The 2005 *XMM–Newton* spectrum showed no evidence of such an outflow, leading to the conclusion that the wind appeared somewhere between 2005 and 2013.

To compare the spectral features around the iron–K α line between the 2005 and 2015–2017 *Chandra* observations, we have made ratio plots by dividing the data by the piled-up power-law model. These are shown in Fig. 7. Since the fluorescent iron–K α line and the absorption edge are not included in the model used for the divisor, their structure can be seen in the ratio spectra. A visual comparison between the two spectra shows that the centre of the iron–K line has not redshifted. In fact, as Table 3 shows, it appears that the line centroid has slightly *blueshifted* between 2000, 2005, and 2015–2017. During the *XMM–Newton* observation in 2005, the line centroid was at 6.39 ± 0.01 keV, lower than the 2005 *Chandra* value of 6.43 ± 0.01 keV .

We think that the most likely explanation for the shift is uncertainties in the gain calibration, and the different chips that were used during each epoch. In the 2000 observations, the AGN was on the S3 chip. In the 2005 observations, the AGN was on I1, with the exception of ObsID 6252, where it was on I3. In all the 2015–2017 observations, the AGN was on I3. According to the *Chandra* Calibration Status Report from 2017 July, the average uncertainty in detector gain is 0.3 per cent. The uncertainty in gain calibration is lowest for the back-illuminated chips, but it can be up to 0.6 per cent on front-illuminated chips at higher focal plane temperatures and at high values of CHIPY. The 2005 observations were all taken with the standard focal plane temperature of $-119.7°$, but the focal plane temperature was $-115°$ during some of the observations between 2015 and 2017. Additionally, the nucleus is positioned at high CHIPY values on most observations. We believe that these factors, combined with the 0.01 keV uncertainty from the fit, can account for the 0.4–0.6 per cent shift between 2000 and the later observations.

However, in all *Chandra* observations the line centroid is significantly higher than during the *NuSTAR* observation, $\mu_{\rm NuSTAR} = 6.34^{+0.03}_{-0.04}$. Therefore, based on the centroid of the iron–K α line, there is no evidence for a redshifted wind component in the *Chandra* spectra.

The absorption edge can clearly be seen in both the 2005 and 2015–2017 spectra. Reynolds et al. (2015) speculate that the absorption edge could be the result of iron–K α absorption in an ionized wind. The fact that the ionized wind is not seen in the *XMM–Newton* data could then be explained by the fact that the absorbing column was significantly higher during that observation in 2005 October. As discussed in Section 4.1, the *Chandra* observations from 2005 show no evidence of a higher absorbing column. Fitting the spectral model to individual ObsID 6252, from September 2005 does not return a higher absorbing column than the average 2005 value. Therefore, if the absorbing column was higher during the *XMM–Newton* observation, it must have increased from roughly 2 to 3 $\times$ 10^{23} cm^{-2} in the month between the observations. This would be a relatively rapid change, especially considering the

Downloaded from https://academic.oup.com/mnras/article-abstract/486/3/3388/5470967 by Universiteit van Amsterdam user on 13 March 2020

absorbing column is around the same value in all *Chandra* and *NuSTAR* observations.

Furthermore, supposing that the fast wind was present in all the *Chandra* data, and is simply related to the amount of absorbing material in our line of sight, it is puzzling why the centre of the iron–K α emission line seen with *Chandra* is inconsistent with that of *NuSTAR*. This alone seems to be the strongest evidence that the fast wind is not present in either 2005 or in 2015–2017. However, this still leaves the exact nature of the absorption edge as an open question.

5 DISCUSSION

5.1 AGN variability in Cygnus A

AGNs are known to be variable on a multitude of time-scales, ranging from hours to years (e.g. Mushotzky, Done & Pounds 1993; Markowitz et al. 2003; González-Martín & Vaughan 2012). In the light curve in Fig. 6, we observe that the X-ray luminosity doubled between 2005 and 2013, and then halved again between 2013 and 2015. In this section, we discuss whether the rise and fall in luminosity can be explained by intrinsic variability of the AGN.

Although most observations have roughly the same duration, on the order of kiloseconds, for the *Chandra* 2015–2017 observations we combined observations over a significantly longer time span. To verify that we are not missing significant variability within that time period, we looked at the 2–10 keV count rates of all the ObsIDs that make up the combined 2015–2017 observation. The count rate is steady with variations of order 10 per cent around the mean. From these observations, there is therefore no evidence that the AGN is highly variable on the time-scale of weeks and months. To explain the increased luminosity seen by *NuSTAR*, we would therefore need to turn to long-term variability.

An extensive study of long-term AGN variability in the 2–10 keV band was carried out by Sobolewska & Papadakis (2009). In the 10 AGN that were studied, a change in luminosity by a factor of 2 seems to certainly be within the realms of possibility. However, this also depends strongly on the properties of the AGN itself. Stochastic modelling of AGN variability shows that the characteristic decay time-scale is larger if the black hole mass is larger (Kelly, Sobolewska & Siemiginowska 2011). For the AGN of Cygnus A, with a black hole mass $M_{\rm BH} = 2.5 \times 10^9$ M$_\odot$ (Tadhunter et al. 2003), this time-scale is of the order of ∼50–1000 d. This means that it could take years for the AGN luminosity to decay back to its mean value. The time between the *NuSTAR* and earliest *Chandra* observations is more than 2.5 yr, so in principle this could have been enough time for the AGN to settle back to its mean luminosity.

Soldi et al. (2014) carried out a long-term AGN variability study with the *Swift* Burst Alert Telescope (BAT). For this study, 66 month light curves (2004 December to 2010 May) in the 15–100 keV band were used. The sample includes Cygnus A. The variability is parametrized as S_V, the sample standard deviation expressed as a percentage of the mean. For Cygnus A, $S_V = 31^{+4}_{-5}$ per cent, compared to the average $\langle S_V \rangle = 24 \pm 1$ for the full sample of 11 radio-loud galaxies.

However, how $S_{V,14-100\rm keV}$ translates to variability between 2 and 10 keV is not directly obvious. At energies above 10 keV, reflection contributes to the total emission, as evidenced by the Compton hump in the *NuSTAR* spectrum around 20–30 keV (Reynolds et al. 2015). The reflection component is expected to be constant because any variability will be smeared out by the light traveltime towards the reflector (Bianchi et al. 2009; Sobolewska & Papadakis 2009). Because the reflection component decreases in strength towards lower energies, the variability at 15–100 keV should be lower than at 2–10 keV.

The observations of Cygnus A before 2000, with *EXOSAT* and *ASCA* show luminosities that are consistent with what we have measured with more recent missions. However, as mentioned before, the relatively low spatial and spectral resolutions make it more difficult to accurately separate the thermal from the non-thermal emission. Fitting a single thermal model to the entire cluster emission would likely leave a hard residual in the spectrum of gas that is hotter than the mean. This hot emission might have been attributed to the AGN, leading to higher measured luminosities. Additionally, the absorbing column is not always well constrained. This means the luminosities measured with these missions are uncertain and that they are consistent with both the idea of a relatively steady AGN, or an AGN doubling or perhaps even tripling its luminosity within a few years.

Given the stochastic nature of AGN variability and the long-term studies of AGN variability at X-ray wavelengths mentioned above, we cannot rule out that the 2013 peak in the Cygnus A light curve is simply the nucleus going through a temporary high-accretion phase.

5.2 The X-ray luminosity upper limit of Cygnus A-2

In Section 3.3, we have estimated an upper limit to the X-ray luminosity of Cygnus A-2, by looking for coincident excess emission in the 2015–2017 *Chandra* observations. The observed 2–10 keV luminosity of the primary AGN in the 2015–2017 *Chandra* observation is $\sim 8 \times 10^{43}$ erg s^{-1}, which gives an upper limit to the observed luminosity of Cygnus A-2 of $\sim 4 \times 10^{42}$ erg s^{-1}. How this translates to intrinsic luminosity depends on the absorbing column and spectral shape of Cygnus A-2. If we assume the spectrum to be an absorbed power law and take the absorbing column to Cygnus A as an upper limit, our upper limit estimate of the 2–10 keV intrinsic luminosity is $\sim 1 \times 10^{43}$ erg s^{-1}.

One of the scenarios that Perley et al. (2017) proposed is that Cygnus A-2 is a steadily accreting secondary AGN. If the radio emission comes from accretion mechanisms, it implies a highly variable AGN, because of the non-detection of Cygnus A-2 in earlier radio observations. Based on the luminosity of the infrared point source that coincides with Cygnus A-2 (Canalizo et al. 2003), this black hole would be accreting at far below the Eddington limit. This means it is expected to lie on the Fundamental Plane for sub-Eddington accreting black holes, given in Plotkin et al. (2012) as

$$\log L_{\rm X} = (1.45 \pm 0.04) \log L_{\rm R} - (0.88 \pm 0.06) \log M_{\rm BH} - 6.07 \pm 1.10. \quad (1)$$

In equation (1), $L_{\rm X}$ is the X-ray luminosity between 0.5 and 10 keV, $L_{\rm R} = (\nu L_\nu)_{5\rm GHz}$ the radio luminosity, and $M_{\rm BH}$ the mass of the black hole in solar mass. If we assume a spectrum with a photon index of $\Gamma = 1.4$, similar to the primary AGN, $L_{0.5-10} \sim 1.2 \times 10^{43}$ erg s^{-1}.

Although no 5GHz observations of Cygnus A-2 were reported on by Perley et al. (2017), we assume $F_{5\rm GHz} = 3.5$ mJy by extrapolating the optically thin spectral model in their fig. 2. This results in a radio luminosity $L_R = 1.3 \times 10^{39}$ erg s^{-1}, and a lower limit to the black hole mass of 4×10^8 M$_\odot$.

Perley et al. (2017) have previously noted two constraints to the upper limit of the Cygnus A-2 black hole mass: first, no dynamical disturbances are observed from IR spectroscopy at the location of Cygnus A-2, implying a mass significantly lower than the mass of the primary black hole (∼2.5×10^9 M$_\odot$, Tadhunter et al. 2003).

Downloaded from https://academic.oup.com/mnras/article-abstract/486/3/3388/5470967 by Universiteit van Amsterdam user on 13 March 2020

The intrinsic scatter of the FP is given in Plotkin et al. (2012) as $\sigma_{\rm int} = 0.07 \pm 0.05$ dex. This means the lower limit that we find can potentially be a little bit lower, but not by a significant amount, and is likely to be at least $10^8 M_\odot$. This is a significant fraction of the black hole mass of the primary AGN. Additionally, the $L_{\rm R}-M_{\rm BH}$ relationship (Franceschini, Vercellone & Fabian 1998), and the pre-flare upper limits to the radio flux density imply a black hole mass $M_{\rm BH} \sim 10^8 M_\odot$, which is inconsistent with our *lower* limit of 4×10^8 M$_\odot$.

Lastly, an estimate for the black hole mass can be obtained from the infrared luminosity of Cygnus A-2 during the 2003 *Keck* observation (Canalizo et al. 2003). This is done by using the scaling relationship between the black hole mass, the 1 μm luminosity, and the width of the Paschen-β broad emission line (Landt et al. 2013, equation 2). Although neither of these values is reported in the paper, the $\nu L\nu$ luminosity at 2 μm is given as 1.7×10^{41} erg s^{-1}. Using this as an upper limit, and assuming a broad Paβ line with a FWHM of 7500 km s^{-1}, implies a black hole mass of 3.2×10^7 M$_\odot$, an order of magnitude lower than we get from the X-ray estimate. However, it is unclear how long-term AGN variability plays into this scenario. It is possible that in 2003, Cygnus A-2 was still in the process of becoming 'active' and thus had not yet reached its full potential infrared luminosity.

Although none of the above arguments give us hard limits, the result is that the range of possible black hole masses for Cygnus A-2 is very narrow: it would require the X-ray luminosity to be at the upper limit, or for Cygnus A-2 to have an absorbing column significantly higher than 2×10^{23} cm^{-2}, for the black hole mass to be at the lower end of the Fundamental Plane due to intrinsic scatter, and for the $L_{\rm Radio}$–$M_{\rm BH}$ correlation to be off by a factor of a few. Therefore, although Perley et al. (2017) favoured the explanation of Cygnus A-2 as an accreting black hole, the lack of X-ray flux seems to argue against this idea. We therefore turn to the alternative scenario of Cygnus A-2 as a TDE, which we discuss in the following section.

5.3 Cygnus A-2 as a TDE

As an alternative to a steady accretion scenario, Cygnus A-2 could have suddenly increased in brightness through a TDE. This would more naturally explain the absence of detectable X-ray emission in the 2015–2017 *Chandra* observations: not all TDEs emit X-ray radiation, and when they do the X-ray emission typically fades on a scale of weeks to months (e.g. Auchettl, Guillochon & Ramirez-Ruiz 2017). While the TDE rate in an average galaxy is estimated to be of the order of 10^{-4}–10^{-5} yr^{-1}, analytical modelling shows that supermassive black hole binary systems may perturb stellar orbits around them enough to yield a significantly higher disruption rate of up to 10^{-1} yr^{-1} (Liu & Chen 2013). The recent discovery of a TDE in an ultra-luminous infrared galaxy by Tadhunter et al. (2017) gives some observational evidence that this may be the case. However, it is unclear whether the separation between the primary AGN and Cygnus A-2, a projected offset of 460 pc, is close enough to result in a significant perturbation of the stellar orbits.

Furthermore, we suggest that the peak in 2–10 keV X-ray luminosity in 2013 might be emission from that TDE. The ∼2.5 yr between *NuSTAR* and *Chandra* observations would have been more than enough for the X-ray emission to fade. Radio emission in TDEs has been observed for ∼2–3 yr after the disruption (e.g. Bright et al. 2018), so an initial disruption in late 2012 or 2013 would be consistent with both X-ray and radio observations.

The difference in 2–10 keV luminosity in the Cygnus A light curve between 2013 and earlier observations is around ~ 1–2×10^{44} erg s^{-1}, but these intrinsic luminosities were calculated by using the absorbing column of the primary AGN, $N_{\rm H} \approx 20 \times 10^{22}$ cm^{-2}. If Cygnus A-2 were instead responsible for the increase in X-ray luminosity, the intrinsic luminosity would likely be lower, because the absorbing column would be a lot lower. The sample of TDEs studied in Auchettl et al. (2017) all have absorbing columns which are, although enhanced compared to their Galactic columns, not larger than $\sim 10^{22}$ cm^{-2}. Based on a range of reasonable absorbing column values, we therefore estimate the intrinsic luminosity to be $\sim(0.5$–$1) \times 10^{44}$ erg s^{-1}.

Most X-ray-emitting TDEs radiate the majority of their energy away through soft, thermal X-ray emission from an optically thick disc, below 2 keV. The exception is the rare class of jetted TDEs, such as Sw J1644 + 57 (Burrows et al. 2011; Zauderer et al. 2013) and Sw J2058 + 05 (Pasham et al. 2015). In jetted TDEs, the non-thermal X-ray emission in the 2–10 keV band can reach peak luminosities of 10^{47} erg s^{-1}. Assuming the standard TDE light-curve evolution of $t^{-5/3}$, 2–10 keV luminosities of order 10^{44} erg s^{-1} could be reached after hundreds of days. If the TDE had ever reached a peak luminosity of 10^{47} erg s^{-1}, it would have been brighter than the rest of the galaxy by orders of magnitude, and it seems unlikely that it would not have been noticed by *Swift* BAT, which continuously monitors the full sky. However, the high luminosities in jetted TDE events are a result of the jet's direct orientation toward our line of sight. A slightly different viewing angle could potentially have led to a lower X-ray peak luminosity more comparable to the X-ray luminosity of the primary AGN.

Alternatively, it has previously been shown in the literature that some thermal TDEs also have a non-thermal emission component in the 2–10 keV band, as in the TDE XMMSL1 J0740-85 (Kawamuro et al. 2016; Saxton et al. 2017). This power-law component is thought to be from the hot corona that Comptonizes the thermal optically thick disc emission. In XMMSL1 J0740-85, the 2–10 keV luminosity is $\sim 5 \times 10^{42}$ erg s^{-1}, which is about an order of magnitude lower than what would be required in Cygnus A-2. The TDE in Cygnus A-2 would therefore have to rather bright for a thermal TDE, and it might fall in what Auchettl et al. (2017) identified as the 'reprocessing valley': an observed luminosity gap between the thermal and jetted TDEs. For TDEs of such brightness, any X-rays are expected to be reprocessed into UV and optical wavelengths before escaping the source.

If Cygnus A-2 is a thermal TDE, we would expect there to be a thermal emission component below 2 keV that is more luminous than the non-thermal emission component. *NuSTAR* does not observe at energies below 3 keV, leaving the 2013 *Swift* XRT observation as the only one that could have potentially seen 0.5–2.0 keV emission from the TDE. We therefore compared the *Swift* spectra from 2007 and 2013 between 0.5 and 2 keV. The 0.5–2.0 keV count rate in 2013 is roughly 13 per cent higher compared to 2007.

We first fit an absorbed thermal model to the 2007 spectrum, which yields a temperature of 3.1 keV and an abundance of 0.6 Z$_\odot$. We then fit the same thermal model plus an additional absorbed power law to the 2013 spectrum, fixing all of the parameters of the thermal model to the 2007 values. We also set an upper limit to the additional absorbing column of 10^{22} cm^{-2}. We find that an absorbed power law with $\Gamma = 1.5$ and $N_H = 0.74 \times 10^{22}$ cm^{-2} gives a good fit to the data, with a reduced $\chi^2 = 19/21$. The intrinsic 0.5–2.0 keV luminosity of the power-law component is 1.8×10^{43} erg s^{-1}. These parameters are all roughly consistent with a TDE spectrum. It is also important to note that the observed rise in 0.5–2.0 keV could

Downloaded from https://academic.oup.com/mnras/article-abstract/486/3/3388/5470967 by Universiteit van Amsterdam user on 13 March 2020

not have been caused by the primary AGN, unless the absorbing column was significantly lower during those observations. However, from the concurrent *NuSTAR* observation in 2013 we know that this is not the case, further supporting the idea that the rise in X-ray luminosity in the *Swift* and *NuSTAR* spectra is connected to Cygnus A-2.

Radio emission has been observed from only six TDEs so far. In all of the jetted TDEs, like the aforementioned Sw J1644+57 and Sw J2058+05, as well as Sw J1112.2 (Brown et al. 2017), 5GHz radio luminosities of 10^{40}–10^{42} erg s^{-1} have been observed. In these events, the radio emission, like the X-ray emission, is thought to arise from the relativistic jets that are oriented towards our line of sight. In three other thermal TDEs, radio emission has been observed with luminosity ranges of 10^{37}–10^{39} erg s^{-1}. The origin of this emission is uncertain, although several models exist, such as transient jets (van Velzen et al. 2016) and non-relativistic winds (Alexander et al. 2016). The radio luminosity at 5 GHz of Cygnus A-2 is $\approx 6 \times 10^{39}$ erg s^{-1}. It is worth noting that the radio luminosity, like the X-ray luminosity, falls right in the middle of a bi-modal luminosity distribution, between the jetted and thermal TDEs. This suggests that if Cygnus A-2 is a TDE, it is unlike previously observed TDEs.

As we have shown in Section 4.5, we see no evidence in the *Chandra* data for the fast, ionized wind that *NuSTAR* detected in 2013. Similar types of outflow have been detected in the TDEs J1521+0749 (Lin et al. 2015) and ASASSN-14li (Kara et al. 2018). They are interpreted as warm absorbers that are fast-moving, with speeds of $\sim 0.12c$ and $\sim 0.22c$, respectively. Additionally, both outflows were detected to be ionized, with $\log \xi \sim 2$–3 erg cm s^{-1}. This resembles the outflow in the *NuSTAR* observation, with a velocity of $\sim 0.06c$ and $\log \xi \sim 3.2$. The *NuSTAR* data also suggests a second wind component with $v \sim 0.16c$, although this component is very poorly constrained.

In ASASSN-14li, the outflow was not detected a year later, suggesting these outflows are naturally short-lived and stop once the accretion rate drops back below the Eddington rate. The time-scale of approximately a year is consistent with the *Chandra* non-detection of the wind a few years after *NuSTAR*.

For the outflow to exist in the first place, it must be super-Eddington. Reynolds et al. (2015) calculated the kinetic energy flux of the wind was to be $L_K > 1.7 \times 10^{45}$ erg s^{-1}. This is below the bolometric luminosity of the primary AGN. However, in a black hole a few orders of magnitudes less massive, this kinetic energy flux well be super-Eddington.

6 CONCLUSION

The absence of X-ray emission from Cygnus A-2 exceeding 5 per cent of the emission from the primary AGN in 2015–2017 *Chandra* observations presents a new constraint on the origin of the transient. In particular, if Cygnus A-2 is a steadily accreting black hole, we would expect its X-ray flux to exceed this limit, unless it is either implausibly massive, $\sim 10^{8-9} M_\odot$, or if the absorbing column is significantly higher than the primary AGN at 2×10^{23} cm^{-2}. In the latter case, the intrinsic luminosity could be a few times higher than the upper limit that we have set.

The lack of X-ray radiation is more naturally explained if Cygnus A-2 is the radio afterglow of a destructive event. Perley et al. (2017) discuss the possibility of a supernova, although the high radio luminosity, the spatial correlation with a previously detected infrared point source, and the lack of variability over the year that the source was monitored with the VLA are all difficult to explain with supernova models. They therefore favour the explanation of a TDE in an offset, secondary AGN. A TDE scenario would not require the secondary black hole to be as massive as in a steadily accreting black hole scenario. Although TDEs are quite rare, 460 pc separation between the primary AGN and Cygnus A-2 might be enough to significantly enhance the average disruption rate of 10^{-4}–10^{-5} yr^{-1} galaxy^{-1}.

The X-ray light curve of the AGN of Cygnus A that we have constructed in this work shows that the 2–10 keV luminosity has been fairly steady since at least 2000, with the exception of 2013, when the luminosity was twice as high. Although it is possible that the luminosity increase can be attributed to stochastic variability that is inherent to AGN, we suggest that Cygnus A-2 might instead have been responsible for this extra X-ray emission. We therefore investigated a TDE model for Cygnus A-2 based on the X-ray observations. To explain the 2–10 keV emission, the TDE would either have to be a powerful, jetted TDE, or a thermal TDE with a hot corona Comptonizing thermal disc emission and re-emitting it as non-thermal power-law emission.

The observed 2–10 keV luminosity increase, of 0.5–1×10^{44} erg s^{-1}, falls in the gap between typical luminosities for a thermal TDE with a non-thermal component (10^{41}–10^{43} erg s-1) and a jetted TDE ($10^{46} - 10^{48}$ erg s^{-1}). Similarly, the radio luminosity, which at 5 GHz is 5×10^{39} erg s^{-1}, falls in between the 10^{37} and 10^{39} erg s^{-1} luminosity range for thermal TDEs, and the 10^{40}–10^{42} erg s^{-1} luminosity range for jetted TDEs. Cygnus A-2 would therefore either have to be a particularly powerful thermal TDE, or particularly faint jetted TDE, perhaps because of a larger viewer angle towards the jet.

We have observed a small increase in 0.5–2.0 keV luminosity in the *Swift* XRT spectra between 2007 and 2013. This increase could not have been caused by the AGN itself, if the absorbing column is indeed as large as measured in 2013 by *NuSTAR*. Although the *Swift* data are not very constraining, it suggests a connection between the 2013 X-ray observations and Cygnus A-2. The detection of the fast, ionized wind in the 2013 *NuSTAR* data, and the non-detection with *Chandra* in 2015, can also be explained by a TDE, as these have been known to launch short-lived fast ionized winds.

The sparsity of X-ray data around 2013, other than the *NuSTAR* and *Swift* observations discussed in this paper, make a more detailed X-ray analysis difficult. Additional observations between 2013 and 2015 could have confirmed whether the post-2013 light curve follows a TDE-like slope. Unequivocal proof that the X-ray emission in 2013 came from a TDE might therefore be out of reach. However, future X-ray observations of the AGN could potentially determine whether the X-ray luminosity rises again, or if perhaps the wind detected by *NuSTAR* has reappeared. If so, then this would imply that the X-ray luminosity peak and the fast wind, are recurring behaviour of the AGN rather than a unique event like a TDE. Continued monitoring with the VLA and the VLBA should be able to confirm whether Cygnus A-2 is indeed a TDE.

ACKNOWLEDGEMENTS

Support for this work was provided by the National Aeronautics and Space Administration through Chandra Award Number GO5-16117A issued by the *Chandra* X-ray Observatory Center, which is operated by the Smithsonian Astrophysical Observatory for and on behalf of the National Aeronautics Space Administration under contract NAS8-03060. This work made use of data supplied by the UK Swift Science Data Centre at the University of Leicester. This research has made use of data, software and/or web tools obtained

Downloaded from https://academic.oup.com/mnras/article-abstract/486/3/3388/5470967 by Universiteit van Amsterdam user on 13 March 2020

from the High Energy Astrophysics Science Archive Research Center (HEASARC), a service of the Astrophysics Science Division at NASA/GSFC and of the Smithsonian Astrophysical Observatory's High Energy Astrophysics Division.

REFERENCES

Alexander K. D., Berger E., Guillochon J., Zauderer B. A., Williams P. K. G., 2016, ApJ, 819, L25
Antonucci R., Hurt T., Kinney A., 1994, Nature, 371, 313
Arnaud K. A., Johnstone R. M., Fabian A. C., Crawford C. S., Nulsen P. E. J., Shafer R. A., Mushotzky R. F., 1987, MNRAS, 227, 241
Auchettl K., Guillochon J., Ramirez-Ruiz E., 2017, ApJ, 838, 149
Bianchi S., Piconcelli E., Chiaberge M., Bailón E. J., Matt G., Fiore F., 2009, ApJ, 695, 781
Bright J. S. et al., 2018, MNRAS, 475, 4011
Brown G. C. et al., 2017, MNRAS, 472, 4469
Burrows D. N. et al., 2005, Space Sci. Rev., 120, 165
Burrows D. N. et al., 2011, Nature, 476, 421
Canalizo G., Max C., Whysong D., Antonucci R., Dahm S. E., 2003, ApJ, 597, 823
Davis J. E. et al., 2012, in Takahasi T., Murray S. S., den Herder J. A., eds, Proc. SPIE Vol. 8443, Space Telescopes and Instrumentation 2012: Ultraviolet to Gamma Ray, SPIE, Bellingham, p. 84431a
Davis J. E., 2001, ApJ, 562, 575
Dickey J. M., Lockman F. J., 1990, ARA&A, 28, 215
Franceschini A., Vercellone S., Fabian A. C., 1998, MNRAS, 297, 817
Freeman P., Doe S., Siemiginowska A., 2001, in Starck J.-L., Murtagh F. D., eds, Proc. SPIE Vol. 4477, Astronomical Data Analysis. SPIE, Bellingham, p. 76
Fruscione A. et al., 2006, in Silva D. R., Doxsey R. E., eds, Proc. SPIE Conf. Vol., 6270, Observatory Operations: Strategies, Processes and Systems. SPIE, Bellingham, p. 62701V
Gehrels N. et al., 2004, ApJ, 611, 1005
González-Martín O., Vaughan S., 2012, A&A, 544, A80
Gordon D. et al., 2016, AJ, 151, 154
Harrison F. A. et al., 2013, ApJ, 770, 103
Hinshaw G. et al., 2013, ApJS, 208, 19
Jackson N., Tadhunter C., Sparks W. B., 1998, MNRAS, 301, 131
Kara E., Dai L., Reynolds C. S., Kallman T., 2018, MNRAS, 474, 3593
Kawamuro T., Ueda Y., Shidatsu M., Hori T., Kawai N., Negoro H., Mihara T., 2016, PASJ, 68, 58
Kelly B. C., Sobolewska M., Siemiginowska A., 2011, ApJ, 730, 52
Landt H., Ward M. J., Peterson B. M., Bentz M. C., Elvis M., Korista K. T., Karovska M., 2013, MNRAS, 432, 113
Lin D. et al., 2015, ApJ, 811, 43
Liu F. K., Chen X., 2013, ApJ, 767, 18
Markowitz A. et al., 2003, ApJ, 593, 96
Mushotzky R. F., Done C., Pounds K. A., 1993, ARA&A, 31, 717
Ogle P. M., Cohen M. H., Miller J. S., Tran H. D., Fosbury R. A. E., Goodrich R. W., 1997, ApJ, 482, L37
Pasham D. R. et al., 2015, ApJ, 805, 68
Perley D. A., Perley R. A., Dhawan V., Carilli C. L., 2017, ApJ, 841, 117
Plotkin R. M., Markoff S., Kelly B. C., Körding E., Anderson S. F., 2012, MNRAS, 419, 267
Privon G. C., Baum S. A., O'Dea C. P., Gallimore J., Noel-Storr J., Axon D. J., Robinson A., 2012, ApJ, 747, 46
Reynolds C. S. et al., 2015, ApJ, 808, 154
Sambruna R. M., Eracleous M., Mushotzky R. F., 1999, ApJ, 526, 60
Saxton R. D., Read A. M., Komossa S., Lira P., Alexander K. D., Wieringa M. H., 2017, A&A, 598, A29
Snios B. et al., 2018, ApJ, 855, 71
Sobolewska M. A., Papadakis I. E., 2009, MNRAS, 399, 1597
Soldi S. et al., 2014, A&A, 563, A57
Stockton A., Ridgway S. E., Lilly S. J., 1994, AJ, 108, 414
Tadhunter C., Marconi A., Axon D., Wills K., Robinson T. G., Jackson N., 2003, MNRAS, 342, 861
Tadhunter C., Spence R., Rose M., Mullaney J., Crowther P., 2017, Nat. Astron., 1, 0061
Tadhunter C. N., Metz S., Robinson A., 1994, MNRAS, 268, 989
Turner M. J. L. et al., 1989, PASJ, 41, 345
Ueno S., Koyama K., Nishida M., Yamauchi S., Ward M. J., 1994, ApJ, 431, L1
van Velzen S. et al., 2016, Science, 351, 62
Young A. J., Wilson A. S., Terashima Y., Arnaud K. A., Smith D. A., 2002, ApJ, 564, 176
Zauderer B. A., Berger E., Margutti R., Pooley G. G., Sari R., Soderberg A. M., Brunthaler A., Bietenholz M. F., 2013, ApJ, 767, 152

This paper has been typeset from a TEX/LATEX file prepared by the author.

Downloaded from https://academic.oup.com/mnras/article-abstract/486/3/3388/5470967 by Universiteit van Amsterdam user on 13 March 2020